Neuron, Volume *97*

Supplemental Information

The Sixth Transmembrane Segment Is a Major Gating Component of the TMEM16A Calcium-Activated Chloride Channel

Christian J. Peters, John M. Gilchrist, Jason Tien, Neville P. Bethel, Lijun Qi, Tingxu Chen, Lynn Wang, Yuh Nung Jan, Michael Grabe, and Lily Y. Jan

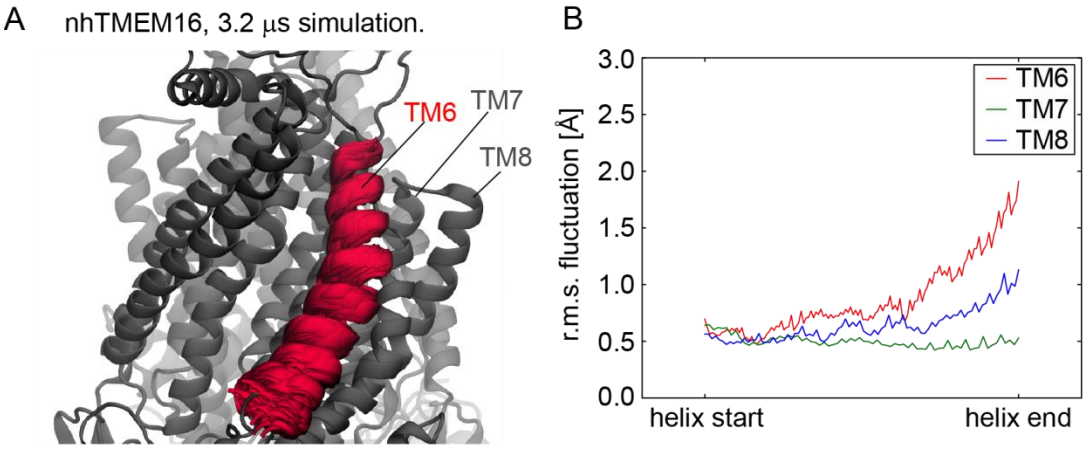

Figure S1. Related to Figure 2. A structural model of TMEM16A based on the nhTMEM16 atomic resolution crystal structure. A. Overlaid positions of the TM6 of nhTMEM16 (PDB: 4WIS) following 3.2 μs of MD simulation. B. RMS fluctuation among predicted coordinates for TM6, 7 and 8 (scaled against helix length) of nhTMEM16 following 3.2 μs of MD simulation.

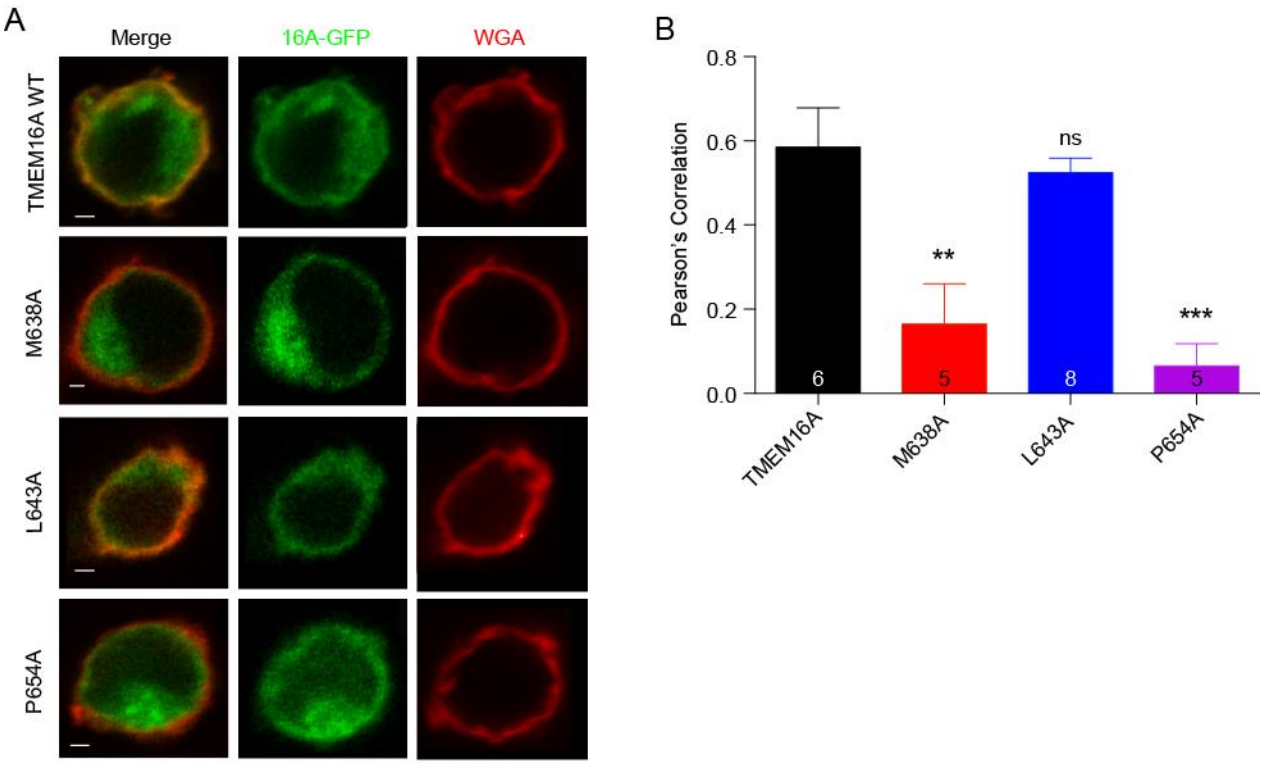

Figure S2. Related to Figure 2. Surface expression comparisons of TMEM16A TM6 mutant constructs with wild-type. A. pEGFP fusion constructs for wild-type TMEM16A and three mutant channels (M638A, L643A, P654A) with currents too small to accurately fit with EC_{50} for Ca^{2+} are expressed in HEK293 cells and co-stained with a rhodamine-tagged wheat germ agglutinin (WGA), a plasma membrane marker, to assess possible defects in surface expression. Scale bars denote 2 μm. B. Pearson's correlations are calculated for green (TMEM16A-pEGFP) and red (WGA) channels in panel A, and average values compared by one-way ANOVA followed by Bonferroni post-hoc test for significance. Data are represented as mean ± SEM.

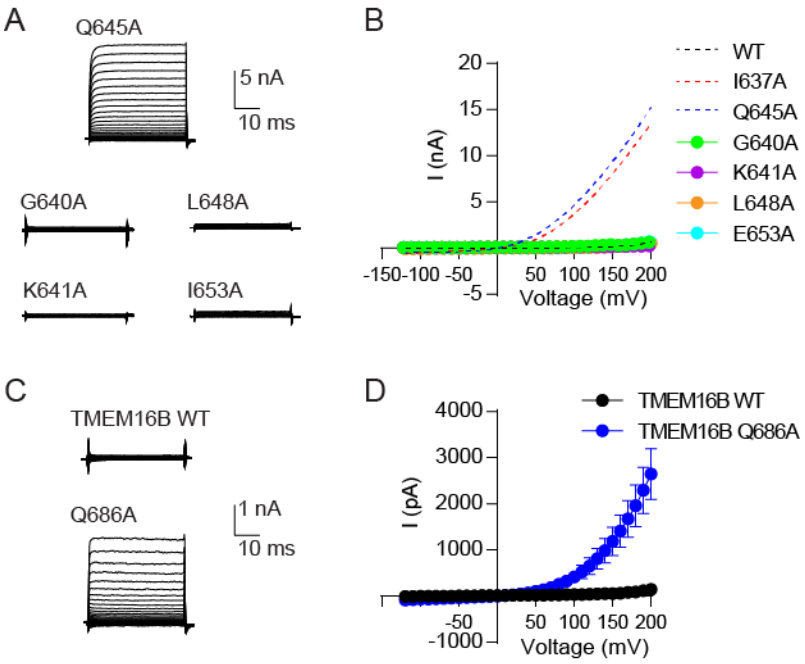

Figure S3. Related to Figure 3. Effects of Ca^{2+}-sensitizing shifting point mutations in TM6 on voltage-dependent currents of TMEM16A and TMEM16B. A. Sample traces for whole cell recordings of TMEM16A mutants G640A, K641A, L648A and I653A, stepped to voltages from -120 to +200 mV in the presence of 0 Ca^{2+} solution are compared with TMEM16A Q645A under the same conditions. B. Current-voltage relationship of TMEM16A G640A (n = 9), K641A (n = 6), L648A (n = 7) and I653A (n = 6) in the presence of 0 Ca^{2+} compared against I637A, Q645A and WT (as in Figure 3B). C. Sample traces for whole cell recordings of TMEM16B and the mutant TMEM16B Q686A (equivalent to TMEM16A Q645A), stepped to voltages from -120 to +200 mV in the presence of 0 Ca^{2+} solution. D. Current-voltage relationship of TMEM16B (n = 7) and TMEM16B Q686A (n = 8) as in panel C. Scale bars in panels A and C apply to all traces. Data are represented as mean ± SEM.

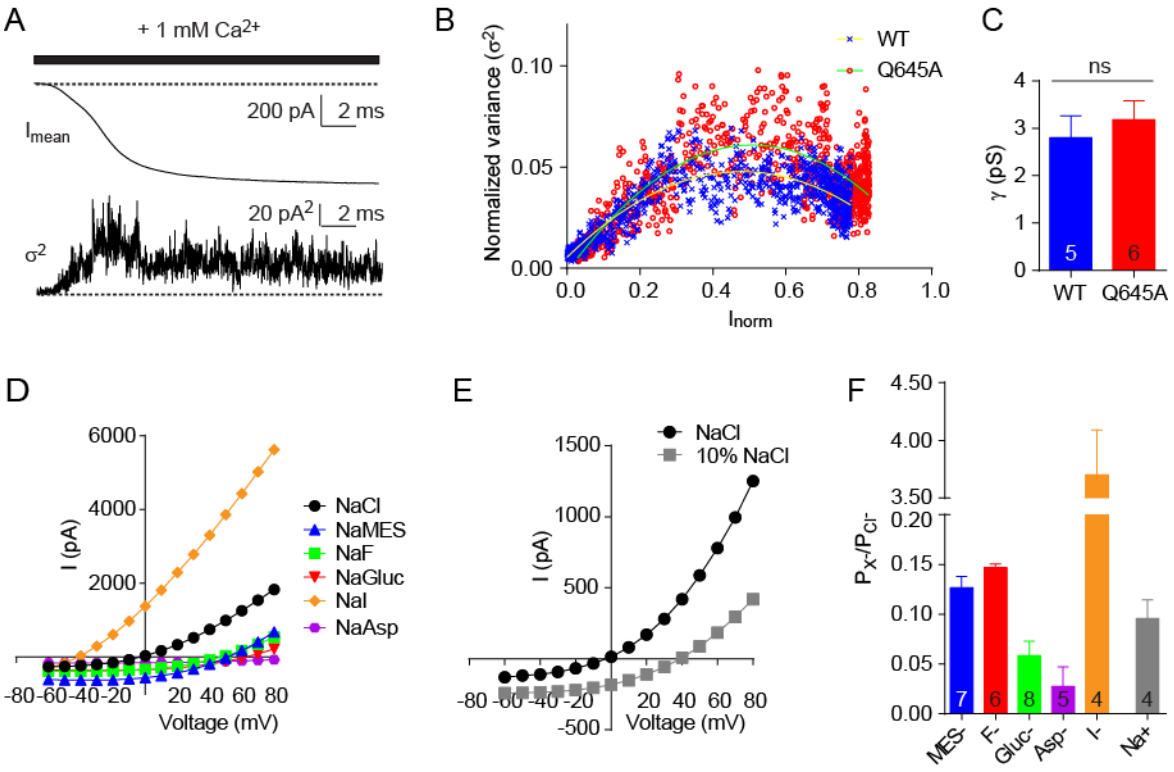

Figure S4. Related to Figure 3. Q645A mutant channels retain conductance and selectivity properties of wild-type channel. A. A sample inside out patch containing Q645A is exposed to a 1 mM Ca^{2+} internal solution, rapidly exchanged from 0 Ca^{2+} solution with a piezo-driven exchanger. Mean current amplitude and variance are shown across time points. B. Variance is normalized to current size, and plotted against it for sample traces for WT and Q645A channels, and the resulting scatter plots fit with Equation S1. C. Single channel conductance is unchanged by this mutant (Student's T-test). D. Current amplitudes from a sample whole cell recording of Q645A, exposed to a series of alternate external anions. E. Sample cell in D was exposed to an osmolality-adjusted solution containing 10% (14 mM NaCl) permeant ion strength. F. Based on experiments in D and E, permeability ratios are calculated for Q645A for all ions shown using Equation S2. All values were compared to 140 mM external NMDG-Cl (normalization point at 1.00) by one-way ANOVA and Bonferroni post-hoc test, and were statistically significantly different, $p < 0.0001$. Data are represented as mean ± SEM.

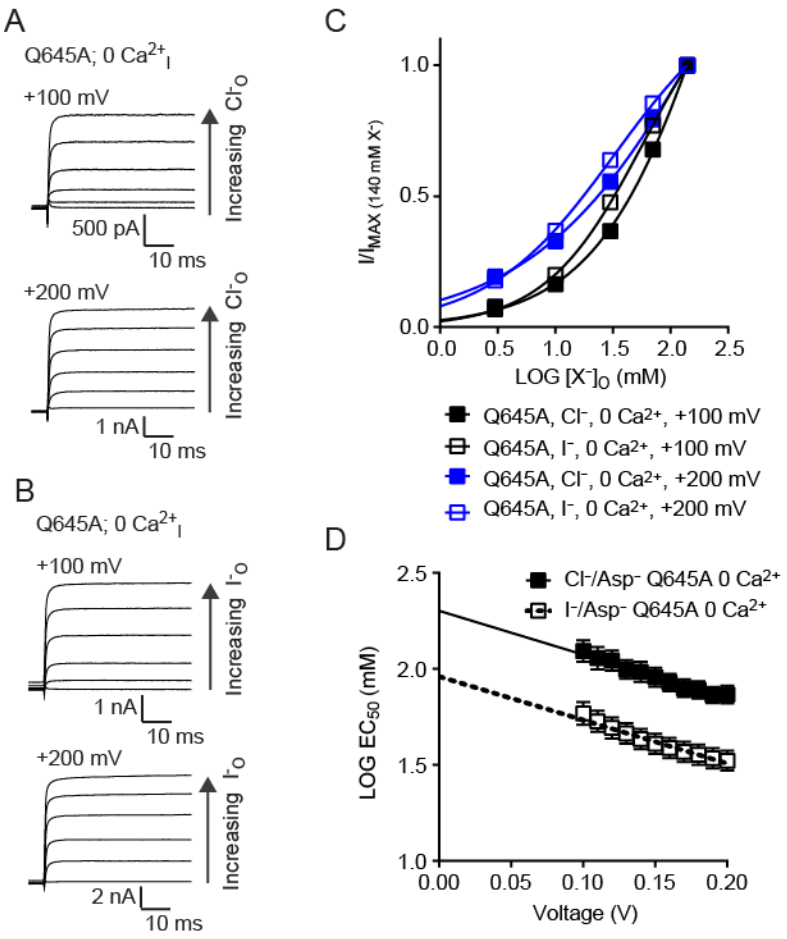

Figure S5. Related to Figures 3-6. A unidirectional current flux voltage clamp assay identifies an anion-binding site near the external pore mouth with state dependent accessibility. A. TMEM16A Q645A channels expressed in HEK293 cells recorded in the presence of 0 intracellular calcium and extracellular chloride ions in increasing concentrations are recorded in whole cell voltage clamp, shown at +100 mV and +200 mV, where intracellular solutions contain aspartate ions in lieu of chloride. B. Q645A channels recorded with extracellular iodide, instead of chloride. C. Concentration-dependence relationships are fit at each voltage tested (+100 mV and +200 mV shown) for current amplitude at increasing concentrations of each external permeant anion. D. LOG EC50 for external anions is plotted for each voltage, and Equation 1 (in Methods) is fit to each set of points. Data are expressed as mean ± SEM and where error bars are invisible, they are contained within the points, n = 6 for both conditions.

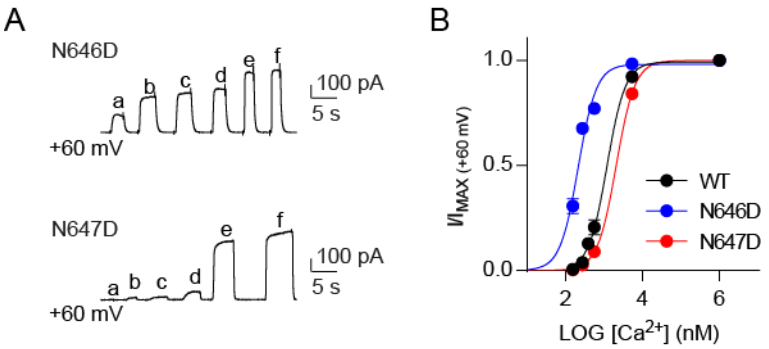

Figure S6. Related to Figure 5. Two adjacent residues have distinct effects on Ca^{2+} sensitivity. A. Sample traces of inside-out patches pulled from HEK293 cells expressing the indicated construct and exposed to a series of increasing Ca^{2+} concentrations at +60 mV. Solutions a-f contained 150 nM, 300 nM, 400 nM, 600 nM, 5.5 μM and 1 mM Ca^{2+}, respectively. B. Graph showing conductance at +60 mV at varying concentrations of Ca^{2+}, as shown in A. A mutation introducing a negative charge at N646D creates a left shift in the calcium dependence of channel activation perhaps through increasing affinity for Ca^{2+} at its binding site. n for these experiments was N646D, 9; N647D, 6. Data are represented as mean ± SEM.

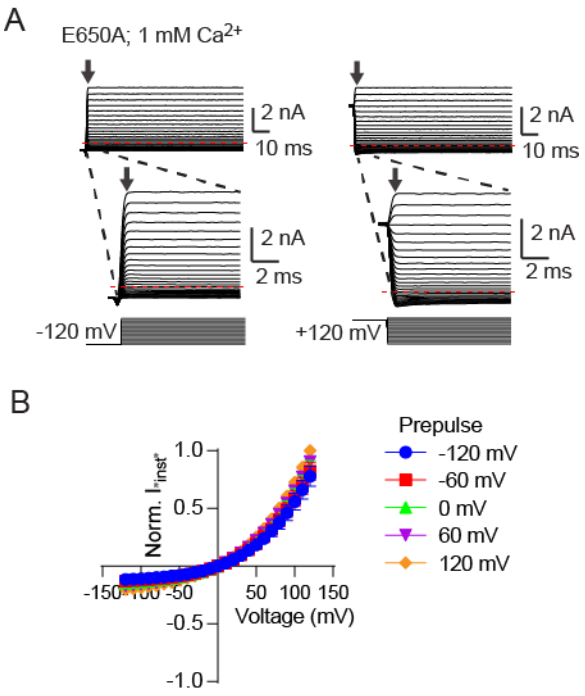

Figure S7. Related to Figure 6. E650A mutant abolishes slow activating currents and instantaneous currents at negative potentials. A. TMEM16A E650A with 1 mM internal Ca^{2+} stepped under voltage clamp from a pre-pulse potential of -120 mV (left) or +120 mV. Inset shows current amplitude immediately after voltage steps. Red dashed lines indicate 0 nA. B. "Instantaneous" current amplitudes from Q645A at voltages from -120 mV to +120 mV after prepulses to the indicated voltages, normalized to amplitude at +120 mV, n = 6. Data are represented as mean ± SEM.